Analysis of Microstructural Inhomogeneities of Ti-Based Alloys Produced via Laser-Based Combinatorial Synthesis

Sheng Li, Shichao Liu, Nicholas J.E. Adkins and Moataz M. Attallah

Interdisciplinary Research Centre (IRC) in Materials Processing, School of Metallurgy & Materials
University of Birmingham, Edgbaston; Birmingham, B15 2TT, UK

Keywords: Laser-Based Combinatorial Synthesis, Ti-Based alloys, Inhomogeneities

Abstract

Combinatorial synthesis from elemental feedstock is a novel way to develop new alloy combinations in a time-efficient approach. In this study, laser-based combinatorial synthesis using elemental feedstock has been used to create small coupons for the Ti-based ternary alloys (Ti-Al-Nb and Ti-Ni-Cu) systems. The aim of this study is to assess the microstructural inhomogeneities of the coupons using quantitative microscopy and X-ray diffraction, and to compare the microstructure to cast alloys. It was found that the microstructural inhomogeneity, in terms of the phase fraction distribution and the chemistry, is insignificant in most alloy combinations. Post-processing heat treatment was generally not essential to obtain an assessment of the utility of the alloy combination, but it can be used to improve the microstructural homogeneity.

Introduction

The demand for high performance Ti-based alloys has dramatically increased due to the versatility of their application in various fields, either for structural or functional purposes. There has been a growing interest in a number of Ti-alloy classes, specifically the Ti-Al-Nb alloys due to their high-temperature performance, the Ti-Ni-based to utilize their shape memory behavior and superelastic properties, and the Ti-Nb-based for their superconducting properties. It can be a tedious task to develop new alloys due to the large number of possible compositional combinations, which calls for more time-efficient and cost-effective methods rather than the conventional one-by-one trial and error method to exploit new compositions. This has led to the development of the so-called "combinatorial synthesis" (CS) approach, which can be used to produce a large number of alloy combinations using a simple process.

Previous work on CS used magnetron sputtering systems to deposit continuous compositional spread-type thin film materials libraries, deposited on Si-wafers substrates [1-3]. Nonetheless, this approach can only produce ~600 nm thin film, which makes it difficult to characterize the microstructure or the properties of the combination. As such, special characterization systems (e.g. nanocalorimetry) would be required to probe the alloy combinations and understand any phase transformations [4]. Additionally, the samples need to be annealed for one hour following sputtering to homogenize the microstructure.

The utility of laser ablation (based on pulsed laser deposition) for CS has also been assessed. The process can produce thin film material combinations relatively easier than sputtering, although

the size of the sample cannot be improved [5], making it difficult to perform mechanical testing. In addition, some of the characteristic are not similar when comparing thin film and bulk materials (e.g. shape memory effect in shape memory alloys [6]). Normally, any scale-up mechanical testing samples have to be made by casting, including vacuum arc melting and vacuum induction melting, which are both known to have a number of limitations (e.g. gravity segregation and the long processing time [7]). Other methods, such as Self-propagating High-temperature Synthesis (SHS) [8, 9], sintering based powder metallurgy [10, 11], and selective laser melting (SLM) [12] were also investigated, but the are occasionally unable to process some alloy combinations that are prone to porosity or cracking formation. Recent work by Polanski *et al.* [13] investigated a powder plus Laser-based CS (LCS) approach, that is based on the laser-engineered net-shaping (LENS) technology. The use of the powder feeding system however limits the process accuracy to be within ± 3 wt. % of the target composition, due to the differences between the powder particles size, flow properties, and melting points.

In this research, a LCS approach is proposed to address the aforementioned issues in the various CS systems, focusing on the microstructural inhomogeneity of the coupons, and highlighting its potential with respect to deposition speed and for the formation of compositionally-graded samples for material libraries [15]. This paper focuses on the analysis of the microstructural inhomogeneities in LCS Ti-based samples.

Materials and Experimental procedures

Laser-based CS technique

A prototype LCS machine was developed, equipped with a CO_2 laser source (maximum power of 1750 W). The system is capable of producing ternary alloys, with a typical compositional accuracy of ± 1% (this and all further chemical compositions in this paper are given in at.%). Deposition is performed in a glove box with a controlled Argon atmosphere (≤30ppm oxygen). The powder feeders in the typical LENS system were replaced by a wire feeding system [14]. The process can be described as being 'high-throughput' since building a Φ10 mm × 45 mm sample can be performed in 20 minutes. As such, it can be used to produce bulk samples for mechanical testing, X-ray diffraction (XRD), or differential scanning calorimetry (DSC). The exact parameters (laser power, vertical feed rate, and material feed rate into the melt pool) are of proprietary nature.

Materials

The feedstock was provided in the form of commercial purity wires (e.g. Ti wire with 99.8% purity and Ni wire with 99.55% purity). A large number of samples were characterized as a part of this project from the Ti-Ni-X and Ti-Nb-X systems. In this paper, a limited number of samples are discussed and analyzed. The samples and their compositions are listed in table 1.

Table 1. Sample code and composition (at. %).

	Ti	Ni	Al	Cu	Nb
Ni50Ti50 (Ni50Ti50)	50	50	-	-	-
Ni52Ti48 (Ni52Ti48)	48	52	-	-	-
Ti50Ni25Cu25 (Ti50Ni25Cu25)	50	25	-	25	-
Nb52Al48 (Nb52Al48)	-	-	48	-	52

The samples were sectioned using wire cutting, mechanically polished to 0.05 μm oxide finish, and etched using Kroll's reagent to reveal the grain structure. The microstructure was investigated using a ZEISS Axioskop 2 optical microscope, as well as a Philips XL30 Scanning Electron Microscope (SEM), equipped with Oxford Inca Energy-Dispersive X-ray Spectroscopy (EDX) system and HKL Channel 5 Electron Backattered Diffraction (EBSD) systems to investigate the microstructural, chemical composition, and texture of the coupons. Phase analysis by XRD was performed using a Philips X'Pert system, equipped with a Cu Kα anode at room temperature. Hardness measurements were performed using a Struers DuraScan hardness tester.

Results and discussions

Microstructural Investigations and phase determine

The optical microscope image of a quarter of the cross section of Ni50Ti50 sample is shown in Fig.1-a. The microstructure of the sample shows three ringed microstructural zones in the sample. The ring at the edge (ring 1) shows a limited fraction of the Ti_2Ni precipitates and some small columnar grains between the edge of the sample. The following zone (ring 2) has the highest precipitate fraction, while the central zone (ring 3) again a reduced precipitates fraction. For the grain size, it was observed that ring 1 showed a mixture of very coarse grains (zone C, up to 1 mm size grains), alongside very fine grains towards the periphery of the coupon. Beyond ring 1, the grain structure is relatively uniform in size, although the grains morphology is relatively heterogeneous. The presence of the Ti_2Ni was also confirmed using XRD, which showed considerable amounts in the as-deposited condition, Fig. 1-b.

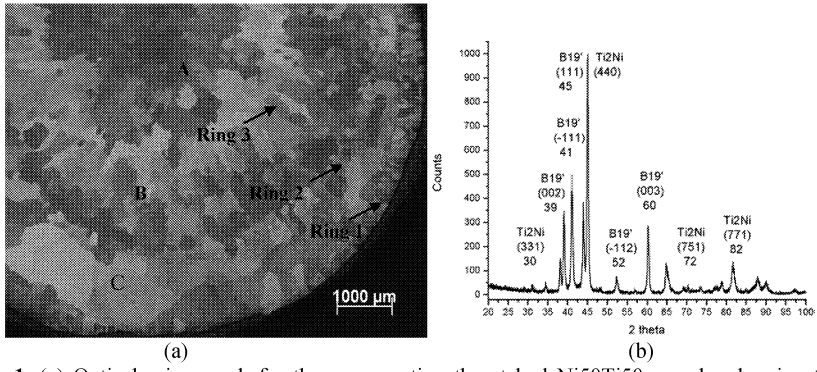

(a) (b)

Fig.1. (a) Optical micrograph for the cross-section the etched Ni50Ti50 sample, showing the three microstructural zones, and (b) XRD pattern for the same sample showing the present phases (B19′ and Ti_2Ni).

The XRD data also shows the B19′ martensite phase, in addition to Ti_2Ni. According to the Ti-Ni phase diagram, Ti_2Ni precipitates below 1237 K while TiNi solidifies at 1583 K [16, 20]. Neither $TiNi_3$ nor Ti_3Ni_4 precipitates were found, which means the composition did not vary due to the chemical segregation to be in the Ni-rich side of the phase diagram. To quantify the Ti_2Ni volume fraction, several images were taken from the various regions in the coupon. It was found that the microstructure showed considerable amounts of Ti_2Ni, which is expected to form under

equilibrium solidification conditions, as shown in the Ti-Ni phase diagram, Fig. 2. The area fraction of the Ti_2Ni particles was found to locally vary between ~2.5% to 21%, with a total average area fraction of 9.8%, as summarized in Table 2. Solution (homogenization) heat treatment can be performed (typically at 1273 K for 2 hr) to eliminate the Ti_2Ni precipitation, so that the homogeneity and the shape memory performance will be improved [19].

Table 2. Area fraction distribution of precipitation in Ni50Ti50 sample.

Regions	A	Ring 3	B	Ring 2	C	Ring 1	Total/Average
Area fraction of regions (%)	24.2	16.2	39.7	4.9	13.3	1.7	100.00
Precipitation area fraction (%)	9.2	2.5	11.3	21.6	11.4	5.8	9.8

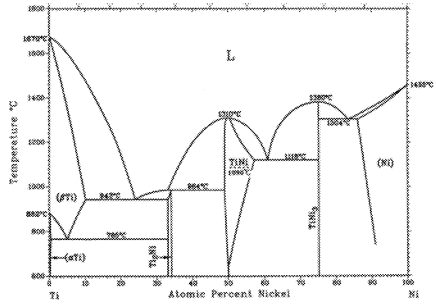

Fig. 2. Ti-Ni phase diagram [16]

By observing the microstructure along the longitude section of the Ni50Ti50 sample, it was observed that columnar grains existed in center vertically along the deposition direction, whereas between center and edge tilt toward center but still columnar in shape, Fig. 3. On the other hand, some evidence of remelting between the successive build layers was observed, which is similar to the remelting patterns typically observed in SLM or LENS process. Remelting is typically associated with a degree of chemical segregation.

To explain the microstructural development, it is essential to consider the details of the process by which the deposition process happens. The molten metal droplets spread on the substrate, which is at room temperature. Nonetheless, the laser beam stays switched on throughout the process, which would keep the melt pool at a high temperature. The build is also surrounded by the argon atmosphere in the glove box, which will keep the periphery of the build at lower temperatures, and exposing it to rapid cooling rates, compared to the central parts which are aligned with the centre of the laser beam, exposing them to further heating. Due to the relatively high cooling rates at the external rings, only a limited amount of the Ti_2Ni is observed, which is also reflected in the occasional presence of coarser grains. At the internal regions, the interaction of the relatively slower cooling rates, combined with solute rejection from the external ring might have led to the formation of a higher fraction of the Ti_2Ni precipitates. The highest

precipitates fraction in ring 2 can be attributed to the equilibrium partition coefficient value difference in Ti (0.46) is much lower than Ni (0.81), which means the segregation tendency of Ti is higher than Ni during solidification [17]. Comparing the longitude section of the Ni50Ti50 sample (Fig. 2-b) with vacuum arc melting Ti50Ni50 sample, the microstructures appear to be similar [18], which suggests that the cooling rates are similar between these two processes. The grain size of the LCS sample is generally finer but quite heterogeneous in size distribution compared to the arc melting samples. In arc melting, up to 6 re-melt cycles are sometimes required to ensure the homogeneity of the sample. On the other hand, laser combinatorial synthesis can not only produce much larger sample, but also build much faster than vacuum arc melting.

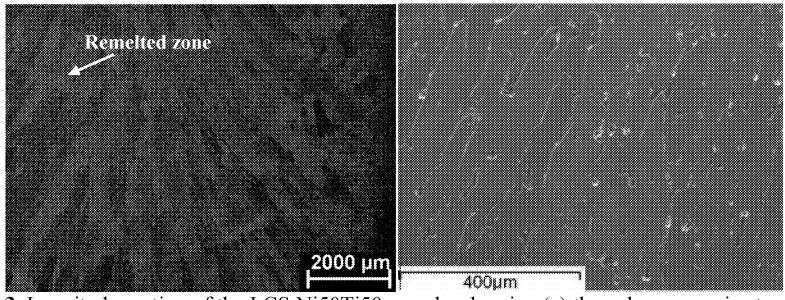

Fig. 3. Longitude section of the LCS Ni50Ti50 sample, showing (a) the columnar grain structure oriented towards the central zone, and (b) SEM micrograph showing the grain structure, surrounded by Ti_2Ni intergranular precipitates.

To assess the crystallographic orientation of the builds, a different sample (Ni52Ti48) was mapped using EBSD, Fig. 4-a. The mapping was only performed on the cross section. It is clear that there is an agglomeration of fine grains toward the edge of the sample, which possibly indicates that the peripheral zones of the build experienced rapid cooling rates. Moving towards the centre, the grain structure appears to be larger in size. Additionally, pole figure were constructed for the entire sample, Fig. 4-b and c), which showed that the texture of Ni52Ti48 sample (with the B2 phase TiNi) is relatively random.

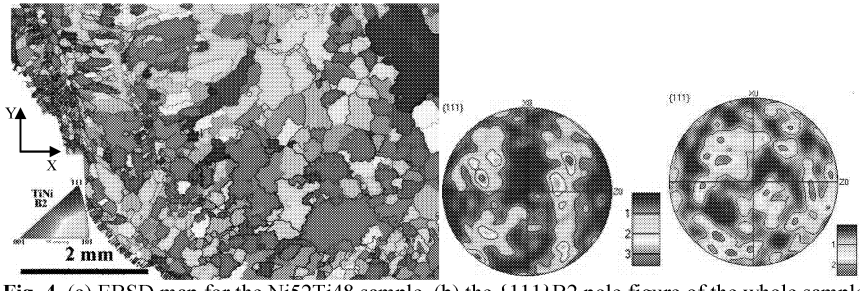

Fig. 4. (a) EBSD map for the Ni52Ti48 sample, (b) the {111}B2 pole figure of the whole sample, and (c) the {111}B2 for the ring external ring area.

Chemical Composition

To assess the chemical homogeneity of the samples, EDX area mapping was used to create a compositional variation contour, using 1 mm × 1 mm area maps, for the Ni50Ti50 sample, Fig. 5-a. It was found that the Ti content varied from 49% to 50.7% (± 0.5%) across the coupon, with the edge showing a higher Ti content at a limited area towards the periphery of the build (previously referred to as ring 1 and region C). Comparing with the outer area, the central region showed a limited high Ti-content, which is believed to be due to centerline segregation. The average Ti-composition for the whole build, however, was 49.9% in Ni50Ti50 sample, which is only 0.1% lower than the target content. Similar patterns were developed for the samples built in ternary systems (Ti50Ni25Cu25, Fig. 5-b) and binary systems with significant differences in melting points between the alloy elements (Nb52Al48, Fig. 5-c). In the ternary systems, the variation in Ti-content was relatively larger (49.7% to 55.5%), and similarly for Al in the NbAl system (42.9% to 48.7%). Nonetheless, typically the variation does not exceed ±2% from the target content, except for local variations towards the edge or the centre of the samples. It is expected that post-deposition homogenization may be required for some of these conditions to eliminate any chemical inhomogeneity in the samples.

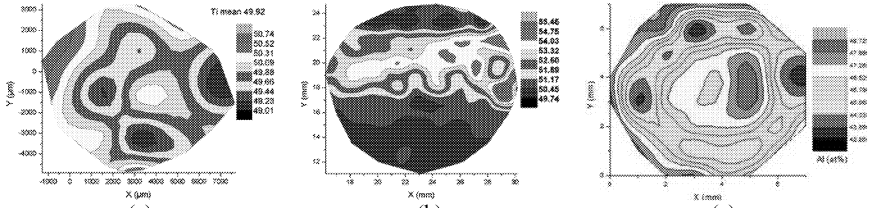

(a) (b) (c)

Fig. 5. Compositional variation contours for the (a)Ti in the Ni50Ti50 sample, (b) Ti in the Ti50Ni25Cu25 sample, and (c) Al in the Nb52Al48 sample.

DSC

Since the shape memory effect is very sensitive to the chemical composition [20, 21], DSC was used to identify the transformation temperatures for the Ni50Ti50. As shown in Fig. 6, the phase transformation temperatures (TTs) and the heat flowing of the LCS alloy was found to match the TTs in the samples produced by the arc melting method [20, 22], with a A_s of ~60˚C and M_f of ~30˚C.

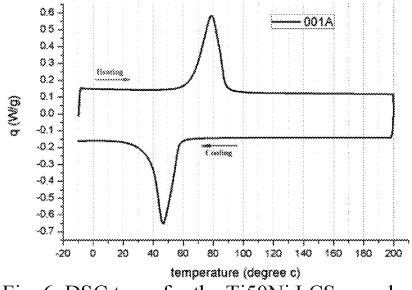

Fig. 6. DSC trace for the Ti50Ni LCS sample.

Conclusions

Samples produced using LCS were studied to assess their microstructural homogeneity, with respect to the grain structure, precipitate structure, chemical composition, and texture. It was found that some local variations were observed in the grain structure and chemical composition, but generally the samples showed no preferential crystallographic orientation in the builds. On average, the chemical composition approaches the target composition, despite the local variations. Post-processing heat treatment was generally not essential to obtain an assessment of the utility of the alloy combination (e.g. the phase transformations), but it can be used to improve the microstructural homogeneity.

References

1. P.J.S.B. Robert Zarnetta, Alan Savan, Sigurd Thienhaus, Alfred Ludwig, Intermetallics 26, 9 (2012)
2. S.T. T. Lehnert, P. Boni, R. Gotthardt, Materials Science and Engineering A 273-275, 4 (1999)
3. A.S. R. Zarnetta, S. Thienhaus, A. Ludwig, Applied Surface Science 254, 6 (2007)
4. P.J.M. Yahya Motemani, Chunwang Zhao, Ming J. Tan, Joost J. Vlassak, Acta Materialia 59, 13 (2011)
5. L.Y. H.D. Gu, K.M. Leung, C.Y. Chung, K.S. Chan, J.K.L. Lai, Applied Surface Science 127-129, 5 (1998)
6. D.K. R. Zarnetta a, C. Zamponi, A. Aghajani, J. Frenzel, G. Eggeler, A. Ludwig, Acta Materialia 57, 9 (2009)
7. S.K.W. K.N. Lin, Scripta Materialia 56, 4 (2007)
8. T.K. K. Kitamura, T. Inaba, M. Tokuda, Y. Yoshimi, Materials Science and Engineering A 438-440, 4 (2006)
9. S.B. N. Resnina, Journal of Alloys and Compounds xxx, 5 (2011)
10. P.B.K. Ning Zhang, J. H. Lindenhovius, B. H. Kolster, Materials Science and Engineering A 150, 8 (1992)
11. J.M. H.X. Zheng, M. Bram, H.P. Buchkremer, D. Stover, Journal of Alloys and Compounds 463, 7 (2008)
12. Y.H. Yongqiang Yang, Weihui Wu, Precess of SPIE 6825, 7 (2008) doi:10.1117/12.757753
13. M.K. M. Polanski, I. Kunce, J. Bystrzycki, International Journal of Hydrogen engergy 38, 13 (2013)
14. M.J. Szidorova1, http://www.enterprise-europe-network.ec.europa.eu/src/matching/templates/completerec.cfm?BBS_ID=176237&org=832&back=true (Ref: 13 NL 1D1D 3RZH), (2013)
15. J.M. Fude Wang, Xinhua Wu, Applied Surface Science 253, 7 (2006)
16. X.R. Kazuhiro Otsuka, Intermetallics 7, 8 (1999)
17. A. GHOSH, Sadhana 26, 20 (2001)
18. A.K. Y. Kabiri, A. Foroozmehr, Vacuum 86, 5 (2011)
19. K.S.F.m.R. Sharghi, Materials and Manufacturing Processes 12 (1), 9 (1997) doi:10.1080/10426919708935124
20. X.R. K. Otsuka, Progress in Materials Science 50, 168 (2005) doi:10.1016/j.pmatsci.2004.10.001
21. E.P.G. J. Frenzel, A. Dlouhy, Ch. Somsen, M.F.-X. Wagner, G. Eggeler, Acta Materialia 58, 15 (2010)
22. F.M.B. Fernandes, K.K. Mahesh, A.d.S. Paula, Thermomechanical Treatments for Ni-Ti Alloys. (2013).